Ex Vivo Gene Therapy Using Patient iPSC-Derived NSCs Reverses Pathology in the Brain of a Homologous Mouse Model

Tagan A. Griffin,[1] Hayley C. Anderson,[1] and John H. Wolfe[1,2,*]

[1]Research Institute of the Children's Hospital of Philadelphia, Philadelphia, PA 19104, USA
[2]W.F. Goodman Center for Comparative Medical Genetics, School of Veterinary Medicine, University of Pennsylvania, Philadelphia, PA 19104, USA
*Correspondence: jhwolfe@vet.upenn.edu

SUMMARY

Neural stem cell (NSC) transplantation is a promising strategy for delivering therapeutic proteins in the brain. We evaluated a complete process of ex vivo gene therapy using human induced pluripotent stem cell (iPSC)-derived NSC transplants in a well-characterized mouse model of a human lysosomal storage disease, Sly disease. Human Sly disease fibroblasts were reprogrammed into iPSCs, differentiated into a stable and expandable population of NSCs, genetically corrected with a transposon vector, and assessed for engraftment in NOD/SCID mice. Following neonatal intraventricular transplantation, the NSCs engraft along the rostrocaudal axis of the CNS primarily within white matter tracts and survive for at least 4 months. Genetically corrected iPSC-NSCs transplanted post-symptomatically into the striatum of adult Sly disease mice reversed neuropathology in a zone surrounding the grafts, while control mock-corrected grafts did not. The results demonstrate the potential for ex vivo gene therapy in the brain using human NSCs from autologous, non-neural tissues.

INTRODUCTION

Neural stem cells (NSCs), the self-renewing precursors of neurons and glia within the developing and adult brain, have the potential to serve as delivery vehicles for therapeutics in the CNS. Transplanted NSCs have been shown to migrate, engraft long term, and secrete beneficial levels of exogenous protein (Aboody et al., 2011; Snyder et al., 1995). There are numerous potential sources of transplantable NSCs, and the development of efficacious therapies will depend on improved methods for their derivation and propagation (Conti and Cattaneo, 2010).

Potential sources of NSCs include cell lines, pluripotent stem cell-derived NSCs, and primary NSCs harvested from fetal or adult animals. Some immortalized NSC lines can engraft and migrate extensively (Snyder et al., 1995), but they may have unstable genomes or pose a risk of tumorigenesis (Koso et al., 2012; Mi et al., 2005; Snyder et al., 1995). Protocols for the differentiation of human embryonic stem cells (ESCs) allow for potentially unlimited expansion of transplantable NSCs, but ESC-derived NSCs are generally incompatible with the host immune system (Koch et al., 2009). Primary NSCs derived from the patient would circumvent immune rejection, but are difficult to obtain and have a relatively limited capacity for expansion and engraftment (Chaubey and Wolfe, 2013; Walton et al., 2008; Wright et al., 2006). A compelling potential solution to this problem involves the use of patient-specific induced pluripotent stem cells (iPSCs), which offer a readily obtainable source of immunologically compatible cells that possess the broad expansion and engraftment potential of ESCs (Guha et al., 2013). The combination of iPSC technology, ESC to NSC differentiation methods, and ex vivo gene therapy offers a promising template for treating a wide range of CNS disorders.

Lysosomal storage diseases (LSDs), which are among the most prevalent monogenetic disorders affecting the brain, may be particularly amenable to this strategy (Meikle et al., 1999). Most often the result of a nonfunctional lysosomal hydrolase, LSDs result in the pathological accumulation of various proteins, lipids, and sugars within the cell. Neuropathology is a significant component of most LSDs, and neurons are particularly susceptible to the accumulation of waste products and associated inflammatory processes (Platt et al., 2012). Intravenous enzyme replacement therapy (ERT) is ineffectual in the CNS due to the impermeability of the blood-brain barrier (Augustine and Mink, 2013), and while intrathecal ERT may be efficacious, it requires regular infusions (Kakkis et al., 2004). NSC-based gene therapy is a potential approach to overcome these obstacles. Donor NSCs can secrete therapeutic levels of lysosomal enzymes, which traffic to host cell lysosomes via the mannose-6-phosphate pathway in a process known as cross-correction (Simonato et al., 2013; Snyder and Wolfe, 1996).

Sly disease (MPS VII) is a prototypical LSD with which to test the efficacy of NSC transplantation due to the availability of cognate animal models and sensitive enzyme assays (Wolfe and Sands, 1996). Here, we utilize the NOD/SCID/MPS VII model (Hofling et al., 2003) to demonstrate an integrated process by which patient somatic cells can be reprogrammed, differentiated into a relevant cell type (NSCs), genetically corrected, and transplanted to yield a therapeutic effect in a mouse homolog of the human disease.
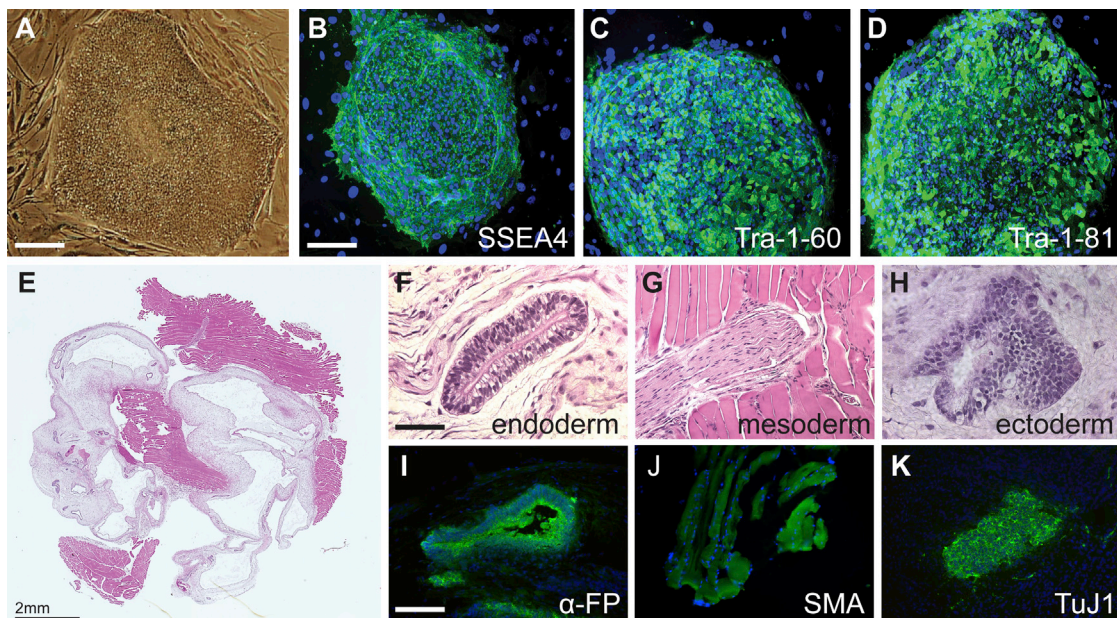
Figure 1. Generation of iPSCs from an MPS VII Patient

Fibroblasts from a female patient with MPS VII (GM02784) were transduced with retroviral vectors expressing the reprogramming factors OCT4, SOX2, KLF4, and c-MYC. A putative iPSC line was isolated and expanded under serum-free conditions on a feeder layer of mouse embryonic fibroblasts.

(A–D) MPS VII iPSC colonies, seen in the phase contrast image (A), expressed markers of pluripotency (B–D).

(E–K) After injection into immunodeficient mice, MPS VII iPSCs formed teratomas (E) that differentiated into the three primary germ layers as shown by H&E-stained sections (E–H) and germ layer-specific marker expression (I–K). α-FP, α-fetoprotein; SMA, smooth muscle actin; Tuj1, βIII-tubulin.

Scale bars represent 200 μm (except in E).

RESULTS

Generation and Characterization of MPS VII iPSCs

Frozen dermal fibroblasts from a patient with MPS VII (GM02784; Coriell Institute) were thawed, expanded, and transduced with vesicular stomatitis virus G protein (VSV-G) pseudotyped retroviral vectors expressing OCT4, SOX2, KLF-4, and c-MYC to initiate reprogramming. Despite the fact that these fibroblasts had been frozen for ~30 years, colonies of ESC-like cells emerged alongside aggregates of partially reprogrammed cells, consistent with previous reports (Chan et al., 2009). One line was selected for further characterization.

To confirm the pluripotency of MPS VII iPSCs, we performed standard in vitro and in vivo assays. The putative MPS VII-iPSC line displayed typical ESC/iPSC-like colony morphology (Figure 1A) and expressed multiple markers of pluripotency, including SSEA4, Tra-1-60, and Tra-1-81 (Figures 1B–1D). Cells injected into immunodeficient mice formed teratomas containing the three primary germ layers. H&E-stained teratoma sections revealed structures typical of endoderm, ectoderm, and mesoderm (Figures 1E–1H), and immunostained teratoma sections were

positive for markers of each lineage (Figures 1I–1K). iPSCs were passaged >40 times with no change in morphology or pluripotency marker expression.

Differentiation of MPS VII iPSC-NSCs

MPS VII and control iPSCs were passaged at least 20 times before being subjected to an adapted NSC differentiation protocol (Koch et al., 2009) (Figure 2). After iPSCs were removed from the mouse embryonic fibroblast (MEF) feeder layer and grown in suspension culture containing fetal bovine serum (FBS), they formed large spherical aggregates. These embryoid bodies were plated and grown in a minimal neural induction medium. A variety of cell types grew outward from the plated aggregates, including many with neurite-like extensions. After approximately 2 weeks, neural tube-like structures began to form on some cell aggregates, consisting of a raised ring surrounding a central lumen (Elkabetz et al., 2008). These rosette structures were isolated and grown as neurospheres for 2 days, after which they were dissociated and plated, yielding an adherent monolayer. No obvious differences were observed between normal and MPS VII iPSCs during the differentiation procedure at any point, and both
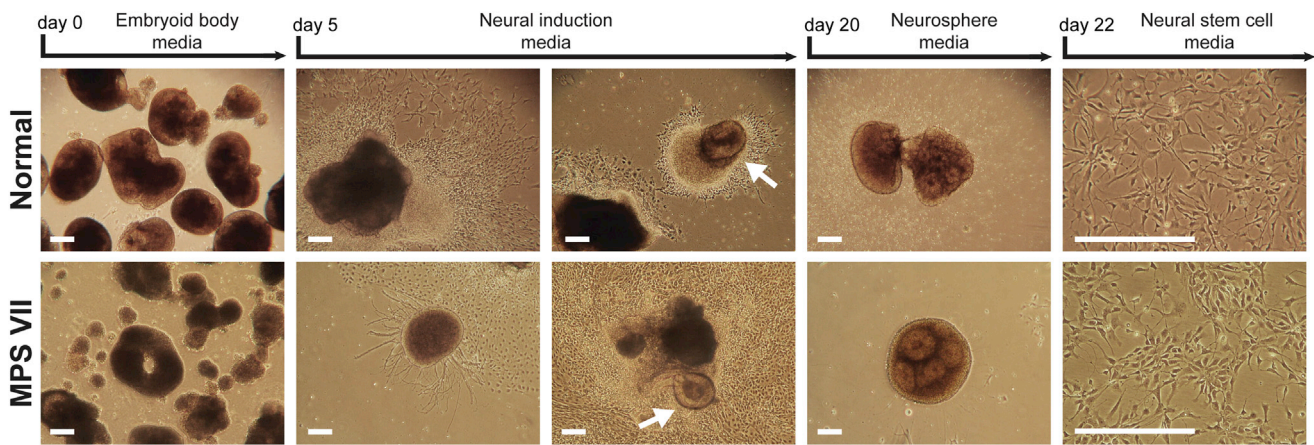
Figure 2. Differentiation of NSCs from MPS VII and Normal iPSCs

Control and MPS VII iPSCs were removed from their MEF feeder layer and grown in suspension culture with FBS for 5 days to induce embryoid body formation. The cell clusters were plated onto poly-ornithine-coated dished and grown in neural induction media. Neural tube-like structures (white arrows) began to appear and were manually isolated at day 20 and then cultured as a suspension in neurosphere media for 2 days. Neurospheres were trypsinized and plated onto poly-ornithine/laminin-coated dishes. Trypsinized cells were passaged as nestin-positive NSCs indefinitely.

Scale bars represent 500 μm.

yielded a relatively homogenous population of putative NSCs (Figure 2).

Characterization of MPS VII iPSC-NSCs

The majority of the iPSC-NSCs (89.9% ± 2.9%) retained expression of the NSC marker nestin (Figures 3A and 3B). The rate of spontaneous differentiation into MAP2-positive neurons (9.5% ± 0.8%) and glial fibrillary acidic protein (GFAP)-positive astrocytes (0.4% ± 0.6%) was low (Figures 3A and 3B). Importantly, no cells expressed the pluripotency marker Tra-1-60 or the reprogramming factor OCT4 (Figures 3A and 3B). The generation and culture of iPSCs from frozen MPS VII fibroblasts and the subsequent differentiation and propagation of iPSC-NSCs did not introduce any gross chromosomal abnormalities, as shown by a normal 46,XX karyotype (Figure 3C). To test the differentiation capacity of these cells, we grew them in terminal differentiation medium without growth factors for 1 month. Differentiating conditions yielded neurons and astrocytes (Figure 3D), as measured by MAP2 (86.4% ± 1.6%) and GFAP (13.9% ± 8.2%) expression, respectively (Figure 3E). The majority of cells (74.8% ± 5.2%) were positive for the inhibitory neurotransmitter GABA, while there was no evidence of tyrosine hydroxylase-positive dopaminergic neurons (Figures 3D and 3E).

Engraftment Potential of GFP-Labeled MPS VII iPSC-NSCs

In order to monitor the in vivo fate of iPSC-NSCs, we first attempted to label cells with GFP using lentiviral vectors with a tropism for multiple neural cell types in vitro and in vivo (Watson et al., 2002). Survival of MPS VII iPSC-NSCs was very low following application of these vectors despite attempts using multiple MOIs, pseudotypes, and transduction conditions. To avoid this apparent toxicity, we used a PiggyBac transposon-based approach instead. The PiggyBac vector expressed a GFP gene and a puromycin resistance gene. The PiggyBac plasmid was electroporated along with a nonintegrating transposase expression plasmid into MPS VII iPSC-NSCs. Two days after electroporation, GFP expression was visible in many transfected cells (Figure 4A). Following a week of puromycin treatment, nearly all cells were GFP positive (Figure 4B) and retained nestin expression (Figure 4C).

To assess the engraftment potential of MPS VII iPSC-NSCs, we intraventricularly injected GFP-labeled cells into neonatal mice, which provide a more hospitable environment for engraftment relative to the adult brain (Snyder et al., 1995). Over 100 NOD-SCID neonates were injected with iPSC-NSCs between passages 15 and 25 with no evidence of deleterious effects. By 1-month post-transplant, cells had engrafted along the rostrocaudal axis of the brain and were primarily found in periventricular regions and white matter tracts (Figure 4E). GFP-labeled MPS VII iPSC-NSCs were also transplanted into NOD/SCID/MPS VII neonates. At 4-weeks post-transplant, the distribution of engrafted cells was similar to the distribution in non-MPS VII NOD/SCID littermates, with cells found predominantly in and around ventricles and white matter (Figure S2). Thus, the disease

MPS VII NSCs
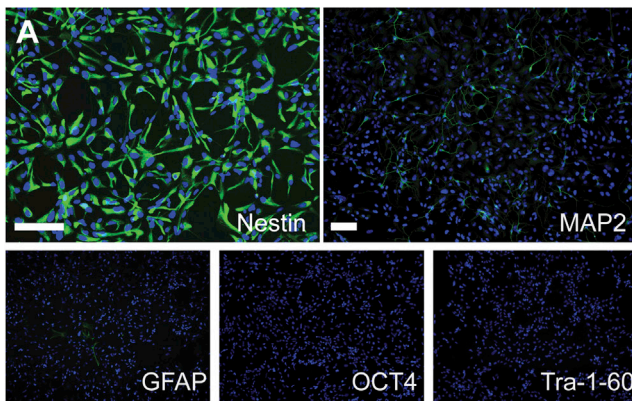
Differentiated MPS VII NSCs

MPS VII NSC Karyotype (46, XX)
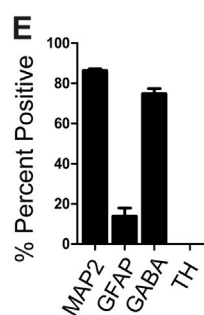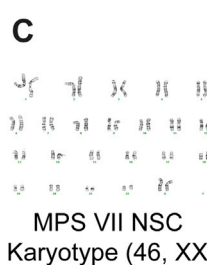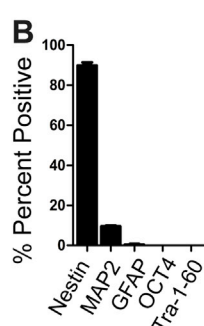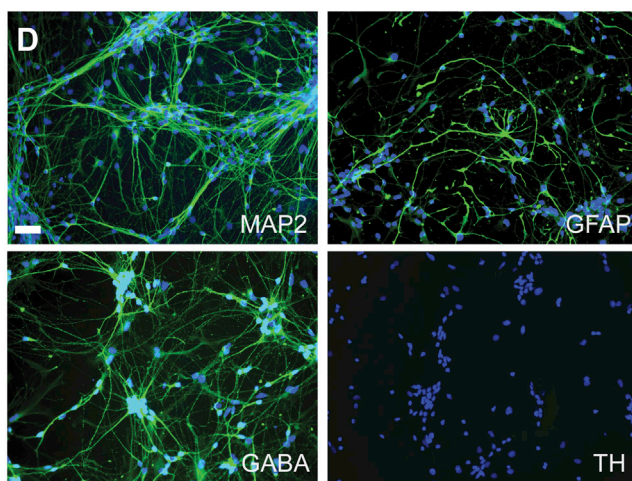
Figure 3. Characterization and Terminal Differentiation of MPS VII iPSC-NSCs

(A and B) MPS VII NSC cultures expressed nestin (89.9% ± 1.5%) and showed low levels of spontaneous differentiation toward neurons (MAP2, 9.5% ± 0.4%) and astrocytes (GFAP, 0.4% ± 0.3%). No cells expressed the reprogramming factor OCT4 or the pluripotency marker Tra-1-60.

(C) MPS VII iPSC-NSCs had a normal 46,XX karyotype.

(D and E) NSCs were subjected to terminal differentiation by the removal of growth factors and the addition of cAMP for 1 month. MAP2-positive neurons comprised 86.4% ± 0.8% of all differentiated cells. The majority of those cells (74.8% ± 2.6%) were GABA-positive, and none of the cells stained positive for the dominergic marker tyrosine hydroxylase (TH). GFAP-positive astrocytes comprised 13.9% ± 4.1% of all differentiated cells.

Data are represented as the mean ± SEM, n = 4 independent cultures. Scale bars represent 200 μm.

did not alter the engraftment properties of the donor cells.

Regardless of location, the engrafted cells expressed nestin and had an immature morphology (Figure 4E, lower). The iPSC-NSCs survived for at least 4 months (Figure 5), with the donor cells predominantly located in the white matter. Engrafted iPSC-NSCs remained in an immature stage even after 4 months in vivo, as indicated by human-specific nestin immunostaining (Figure 5B). Despite their immature phenotype, transplanted iPSC-NSCs quickly exited the cell cycle. At 1-week post-transplant, only a few cells expressed the cell proliferation marker Ki67, and no Ki67-positive cells were seen at 4- or 16-weeks post-transplant (Figure S1).

Therapeutic Potential of Corrected MPS VII iPSC-NSCs

The MPS VII iPSC-NSCs were genetically corrected and introduced into an adult MPS VII host in order to evaluate their therapeutic potential. The iPSC-NSCs were electropo-

rated with a PiggyBac vector expressing the *GUSB* cDNA driven by the CAG promoter. A separate culture of the same passage of NSCs was prepared as a negative control by electroporating them with a mock-correction vector containing the *GUSB* cDNA in the reverse orientation. After puromycin selection, the mock-corrected MPS VII iPSC-NSCs had negligible GUSB activity (1.3 ± 1.3 nmol 4-MU/μg protein/hr) while the corrected cells showed strong GUSB activity (116.8 ± 2.7 nmol 4-MU/μg protein/hr, $p < 0.01$), comparable to an iPSC-NSC line derived from a healthy control (112.3 ± 3.1 nmol 4-MU/μg protein/hr, $p > 0.05$) (Figure 6A).

MPS VII is a progressive disease with extensive pathology present by 2 months of age (Levy et al., 1996; Snyder et al., 1995). Therefore, 2-month-old NOD/SCID/MPS VII mice were injected bilaterally into the striatum with 50,000 corrected MPS VII iPSC-NSCs in one hemisphere and 50,000 mock-corrected cells in the contralateral hemisphere. Animals were sacrificed 1 month later. Engrafted cells survived,
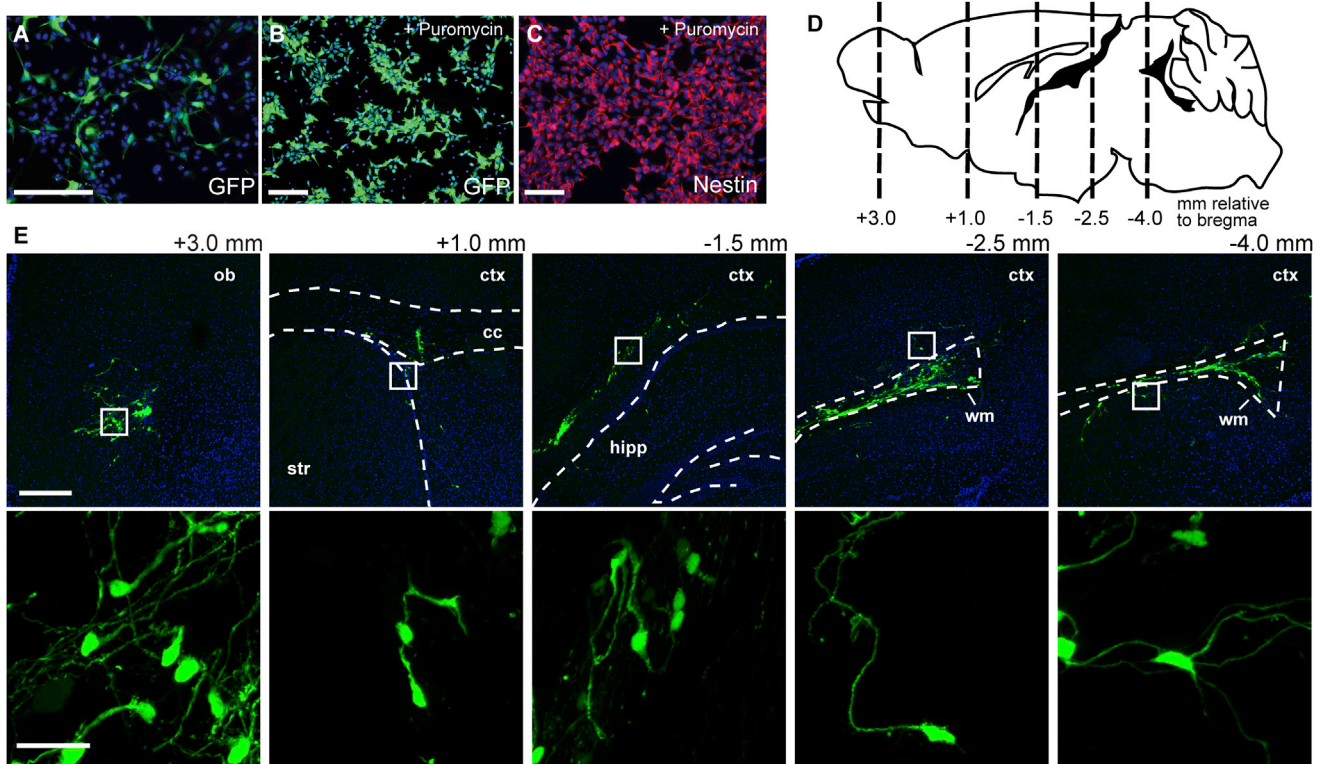
Figure 4. GFP Labeling and Distribution of Engrafted MPS VII iPSC-NSCs

(A) A PiggyBac transposon-based plasmid encoding GFP and a puromycin resistance gene was electroporated into MPS VII iPSC-NSCs.

(B) Puromycin was applied for 7 days in order to select for NSCs that had been stably transduced.

(C) MPS VII iPSC-NSCs retained their nestin expression and growth capacity after electroporation and puromycin selection.

(D) 100,000 GFP-labeled iPSC-NSCs were transplanted into the lateral ventricles of neonatal NOD/SCID mice.

(E) At 1-month post-transplant, cells were found along the rostral-caudal axis of the brain, often adjacent to ventricles and within white matter tracts. The areas within the white boxes are enlarged in the bottom, showing the morphology of engrafted iPSC-NSCs.

Scale bars represent 200 μm (A–C), 500 μm (E, upper panels), and 30 μm (E, lower panels). See also Figures S1 and S2.

remained nestin positive, and did not migrate away from the injection site. GUSB enzymatic activity, detected by a histochemical reaction (Snyder et al., 1995), was limited to the injection site of the hemisphere receiving corrected cells (Figure 6B).

To test whether the lack of differentiation and migration was unique to our MPS VII line or to the diseased environment, we transplanted iPSC-NSCs derived from a healthy human control, as well as MPS VII iPSC-NSCs, into NOD/SCID (non-MPS VII) adult mice. At 1-month post-transplant, engrafted cells from both lines remained at the injection site and stained positive for human-specific nestin (Figure S3). This demonstrates that iPSC-NSCs from a normal or a diseased source had the same properties when transplanted into adult brain parenchyma.

To determine whether corrected or mock-corrected MPS VII iPSC-NSCs affected neuropathology in MPS VII mice, we used changes in activated microglia as a marker of neuropathology. Neuroinflammation is a common finding

in neurodegenerative diseases, and microarray analysis of the MPS VII brain has shown that CD68, the major marker of microglial activation, is transcribed at very high levels (Parente et al., 2012). We confirmed via immunostaining that CD68 was highly upregulated in NOD/SCID/MPS VII animals early in the disease process, preceding the appearance of other commonly used markers of neuropathology (Figure S4). CD68-positive microglia were uniformly distributed throughout the MPS VII brain by 3 months of age (Figure 7).

One month following adult transplantation, there was a striking reduction in CD68 immunoreactivity surrounding the corrected MPS VII iPSC-NSC grafts, but not the mock-corrected grafts (Figures 7A and 7B). The density of CD68-positive cells was quantified in a 0.5-mm^2 region of interest (ROI) surrounding each injection tract (Figure 7C). There was a significant difference between the region surrounding corrected grafts (49.2 ± 9.9 cells/mm^2) versus the region surrounding mock-corrected grafts
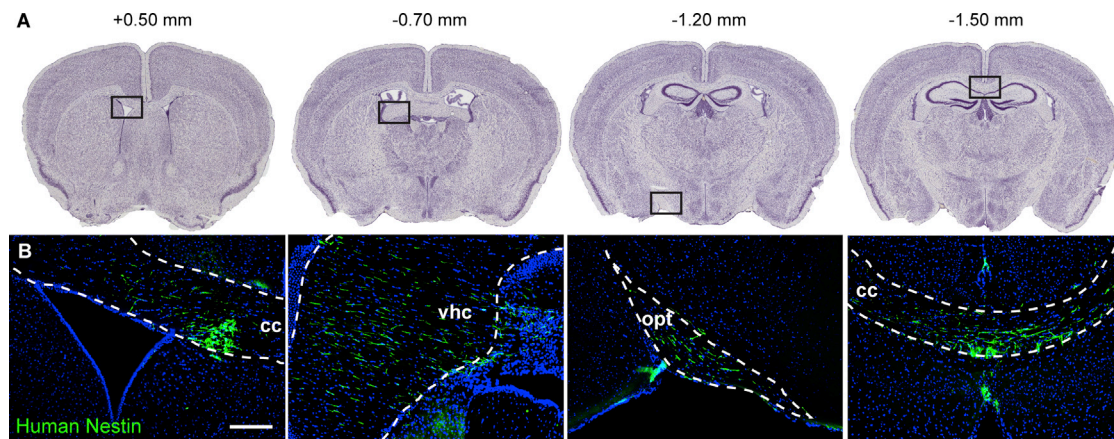
Figure 5. MPS VII iPSC-NSCs Survive and Retain Nestin Expression 4 Months following Intraventricular Injection

The presence of engrafted iPSC-NSCs was revealed by immunostaining 4 months after neonatal transplantation. The highest concentrations were found in and along white-matter tracts.

(A) Black boxes over Nissl-stained coronal sections show the locations of engrafted MPS VII iPSC-NSCs seen below. The location relative to bregma (in mm) is shown above each section.

(B) Engrafted MPS VII iPSC-NSCs remained nestin positive even after 4 months in vivo.

The scale bar represents 200 μm. cc, corpus callosum; vhc, ventral hippocampal commissure; opt, optic chiasm. Nissl-stained sections are from the Allen Mouse Brain Atlas (Allen Institute for Brain Science).

(145.2 ± 13.2 cells/mm^2, $p < 0.0001$) (Figure 7C). There was not a significant difference between the region surrounding mock-corrected grafts and a comparable region of untreated MPS VII striatum (166.1 ± 13.4 cells/mm^2, $p > 0.05$). Immunostaining for CD68 and the pan-microglial marker showed that the microglia in untreated MPS VII mice as well as the microglia surrounding mock-corrected iPSC-NSCs had a distended, amoeboid-type morphology (Figure 7D). In contrast, the region surrounding corrected iPSC-NSCs contained smaller, ramified-type microglia, which closely resembled the microglia in normal control brains (Figure 7D). As a control for the effect of localized GUSB overexpression on CD68-positive microglia in the absence of transplanted iPSC-NSCs, we injected adult MPS VII mice with an AAV-GUSB vector (Passini et al., 2003). At 1-month post-injection, there was localized clearing of CD68-positive microglia around the injection site (Figure S5), similar to that seen after corrected MPS VII iPSC-NSC transplantation.

DISCUSSION

Here we demonstrate the feasibility of ex vivo gene therapy for the treatment of neuropathology accompanying metabolic disease using patient-derived somatic cells from a readily accessible source (e.g., skin biopsy). By reprogramming patient fibroblasts into pluripotent stem cells and subsequently generating genetically corrected tissue-spe-

cific stem cells, we evaluated a therapeutic strategy that can be applied to many genetic diseases affecting the brain. We show, via xenotransplantation into a mouse homolog of the human disease, that such a strategy can reverse pathologic lesions surrounding the engrafted cells.

The success of NSC-based therapy will depend on protocols that yield well-characterized and expandable lines suitable for transplantation. We chose an NSC differentiation protocol for its ability to generate a self-renewing population of relatively homogenous NSCs from ESC and iPSC lines (Falk et al., 2012; Koch et al., 2009). The in vitro characteristics of MPS VII iPSC-NSCs generated here were consistent with reports utilizing similar ESC-based protocols in regards to the immunophenotype and ability to generate predominately GABAergic neurons upon withdrawal of growth factors (Koch et al., 2009).

We found that GUSB deficiency did not compromise the ability of human MPS VII iPSCs to generate embroid bodies or differentiate toward neural lineages, in contrast to a previous report on a mouse MPS VII iPSC line (Meng et al., 2010). Disease-related phenotypes have been reported, in vitro, in iPSCs derived from patients with other LSDs, such as Niemann-Pick type C or MPS IIIB (Bergamin et al., 2013; Lemonnier et al., 2011), and in primary canine MPS VII NSCs (Walton and Wolfe, 2007). However, there was no evidence in our study that the MPS VII iPSC-NSCs or their progeny had a disease-related phenotypic difference in vitro. The GUSB deficiency also did not impair engraftment as we observed no apparent differences in
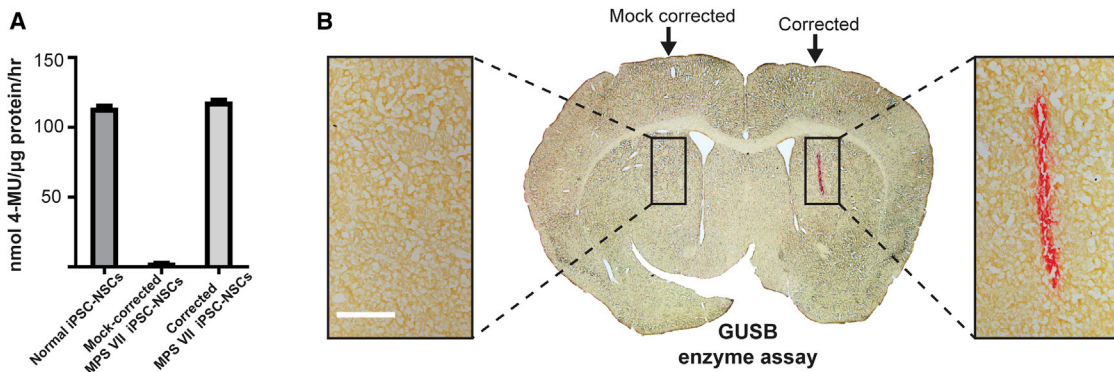
Figure 6. Genetic Correction of MPS VII iPSC-NSCs and Adult Transplantation

iPSC-NSCs were electroporated with a PiggyBac plasmid containing *GUSB* cDNA or a mock-correction vector containing *GUSB* cDNA in the reverse orientation.

(A) Following puromycin selection, GUSB activity in corrected and mock-corrected MPS VII iPSC-NSCs was compared with enzyme activity in NSCs derived from control iPSCs (mean ± SEM, n = 3 independent cultures).

(B) 50,000 cells were injected bilaterally into the striatum of 2-month-old NOD/SCID/MPS VII mice. One hemisphere received corrected MPS VII iPSC-NSCs, and the other hemisphere received mock-corrected MPS VII iPSC-NSCs. At 1 month following transplantation, enzyme activity was present at the injection tract in the hemisphere receiving corrected cells, but not in the hemisphere receiving mock-corrected cells.

n = 4 mice. The scale bar represents 0.25 mm. See also Figure S3.

numbers or distribution of donor NSCs between genetically corrected and mock-corrected MPS VII iPSC-NSCs after transplantation into MPS VII mice.

Transplantation of iPSC-NSCs within the neonatal brain yielded stable engraftment across the neuroaxis for at least 4 months, but only within and adjacent to white matter tracts. Although the precise mechanisms are unclear, NSCs from various sources display a tropism for white matter in both normal and pathological contexts (Carney and Shah, 2011; Gupta et al., 2012; Maciaczyk et al., 2009; Tabar et al., 2005). The affinity for white-matter tracts may be useful for treating leukodystrophies or as a pathway for NSC dissemination. The limited migration of transplanted NSCs within gray matter may be a barrier to widespread delivery for some diseases with global CNS pathology; however, axonal transport can facilitate wider distribution of lysosomal proteins within this group of diseases (Passini et al., 2002).

We transplanted iPSC-NSCs into neonatal mice in order to evaluate their behavior in a more appropriate developmental context. Many cues required for the survival and migration of NSCs are present in neonates, but not in healthy adults (Guzman et al., 2007). We found that iPSC-NSCs engraft widely, but sparsely, which is consistent with neonatal transplants of primary mouse NSCs (Chaubey and Wolfe, 2013). Following transplantation directly into gray matter (adult striatum), the iPSC-NSCs remain localized to the injection tract. As a consequence, microglial pathology was corrected in a zone surrounding the graft, corresponding to the distribution of enzyme in three

dimensions in the brain parenchyma (Taylor and Wolfe, 1997). Thus, substantial improvements to increase the distribution of donor cells within the brain will be needed to deliver the therapeutic enzyme to more areas of the brain to advance clinically relevant NSC therapy further for LSDs.

The engrafted iPSC-NSCs showed very little evidence of differentiation, even 4-months post-transplant. The absence of mature neurons and glia following neonatal and adult transplantation stands in contrast to the proficiency with which iPSC-NSCs are able to undergo terminal differentiation in vitro. This result underscores the need for a better understanding of the factors governing NSC differentiation. However, for use in correcting most LSDs, the differentiation status is not critical, provided that engrafted cells do not cause deleterious effects in the brain. Undifferentiated cells may in fact be advantageous, as inappropriate neurotransmitter release from mature engrafted neurons can be harmful in some settings. One example of this is the graft-induced dyskinesias resulting from cell replacement therapy for Parkinson's disease (Lane et al., 2010).

Gene- and cell-based therapies that successfully deliver lysosomal enzymes in the brain reduce pathology in many animal models of LSD (Simonato et al., 2013). To test whether genetically corrected patient iPSC-NSCs could deliver corrective levels of GUSB, we evaluated pathology in the striatum surrounding engrafted cells in adult MPS VII brains. We assayed disease-associated neuroinflammation as a biomarker, using CD68-positive activated microglia. A microglial contribution to MPS VII pathology was
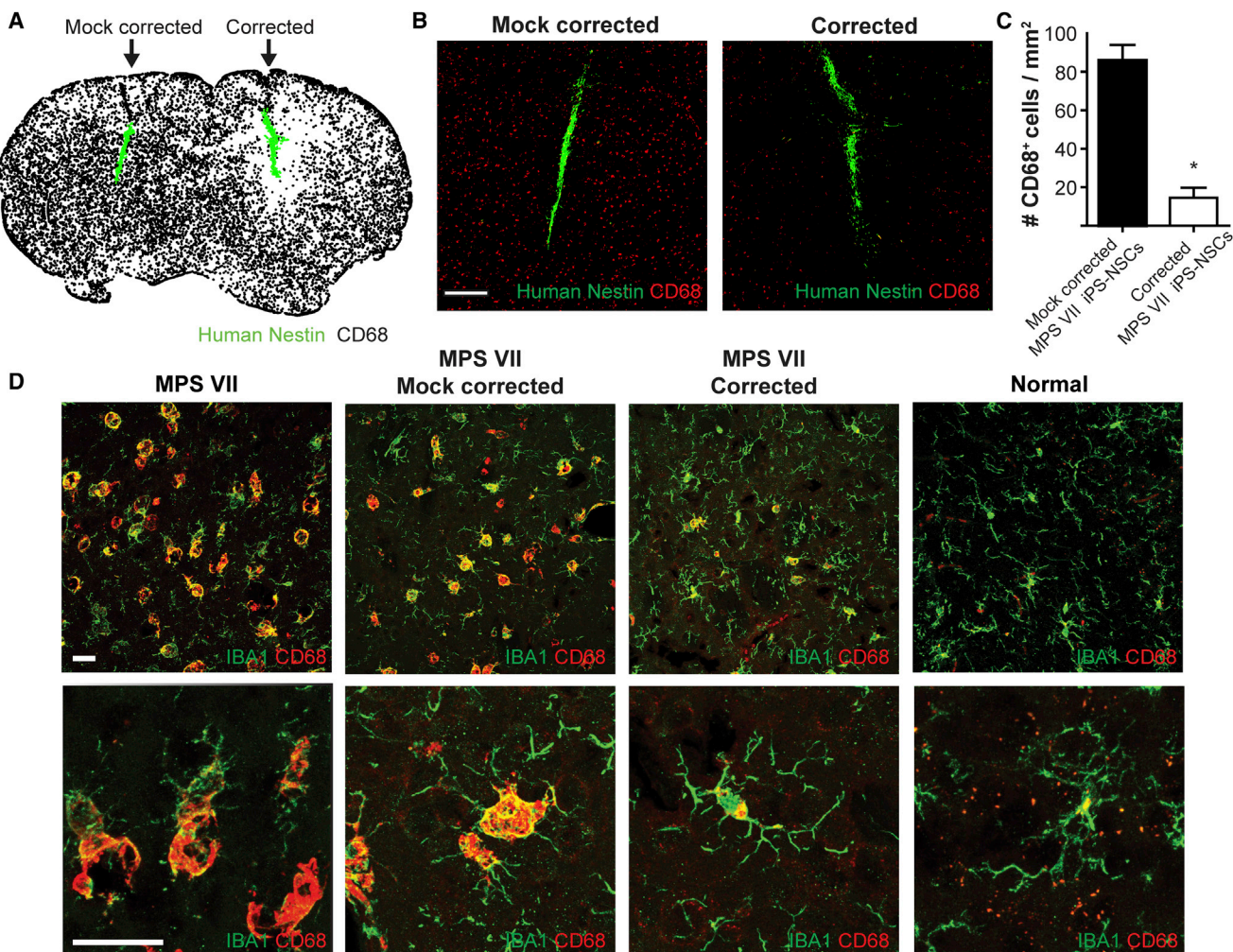
Figure 7. Correction of Microglial Pathology following iPSC-NSC Transplantation

Corrected and mock-corrected iPSC-NSCs (50,000 cells/condition) were injected intrastriatally into the right and left hemisphere, respectively, of adult NOD/SCID/MPS VII mice.

(A) Schematic of a representative coronal section showing engrafted MPS VII iPS-NSCs and CD68-positive microglia at 1-month post-transplantation.

(B) Immunofluorescent images of nestin-positive iPS-NSCs at the site of injection. The region surrounding the corrected MPS VII iPSC-NSCs contained significantly fewer activated microglia than in the region surrounding mock-corrected MPS VII iPSC-NSCs or in a comparable region of untreated MPS VII striatum.

(C) CD68-positive microglia with an area greater than 20 pixels were quantified.

(D) Confocal images of IBA1 and CD68 immunoreactivity in resident microglia. The brains of MPS VII mice showed marked microglial activation, as evident by upregulated CD68 expression and amoeboid morphology. Microglia adjacent to corrected, but not mock-corrected, MPS VII iPSC-NSCs exhibited a ramified morphology and low CD68 expression typical of the quiescent microglia found in normal mice.

Mean ± SEM, n = 3 sections/mouse, n = 4 mice. Scale bars represent 200 μm in (B) and 30 μm in (D). See also Figures S4 and S5.

previously shown via microarray analysis of normal and diseased brains (Parente et al., 2012). Microglia involvement has been well documented in some, but not all, storage diseases, including MPS IIIb and Sandhoff disease (Ohmi et al., 2003; Wada et al., 2000), and activated CD68-positive microglia have been used as a biomarker for correction of pathology (Lee et al., 2007). We show here that microglia are a significant and early component of MPS VII neuropathology. The CD68-positive microglia are particularly useful as a quantifiable biomarker of MPS VII neuropathology because of their distended size, spherical morphology, and uniform distribution.

We observed no differences in the ability to establish grafts between corrected and mock-corrected MPS VII iPSC-NSCs. The diseased area surrounding the mock-corrected grafts was essentially the same as untreated MPS VII brains in the same region, and the activated microglia had a distended ameboid appearance. In contrast, the area surrounding the grafts of the corrected MPS VII iPSC-NSCs had significantly fewer CD68-positive cells, and the remaining microglia were reduced in size and adopted a more ramified-type morphology consistent with the state of resting microglia seen in normal animals.

The lack of benefit derived from mock-corrected grafts indicates that GUSB alone was responsible for correcting the neuropathology, rather than anti-inflammatory or other factors expressed by the iPSC-NSCs themselves. The observation that GUSB overexpression from an AAV vector similarly reduces CD68-positive microglia corroborates the conclusion that GUSB activity is solely responsible for the correction of neuropathology.

The spatially constrained nature of correction following cell transplantation indicates the need for new differentiation protocols or other strategies capable of increasing NSC migration within the brain parenchyma. Overall, our results suggest that a comprehensive strategy involving somatic reprogramming and gene therapy could benefit patients with neuropathology from storage diseases affecting the brain.

EXPERIMENTAL PROCEDURES

Generation of MPS VII iPSCs

Frozen fibroblasts were obtained from a 3-month-old female patient (GM02784; Coriell Institute for Medical Research) with no detectable β-glucuronidase activity. Fibroblasts were maintained in DMEM containing 15% FBS. Reprogramming was performed as previously described with some modifications (Park et al., 2008). Retroviral vectors expressing OCT4, SOX2, KLF4, and c-MYC were produced in 293t cells using the pMXs backbone (courtesy of Dr. Shinya Yamanaka, Addgene plasmids 13366, 13367, 13375, and 17219) and pseudotyped with VSV-G (Takahashi and Yamanaka, 2006). MPS VII fibroblasts were transduced with the reprogramming vectors and after 5 days were split onto mitomycin-C inactivated MEFs. The cells were maintained in iPSC media containing ROCK inhibitor Y-27632 (10 μM; Sigma) until colonies were ready to be picked. Putative iPSC colonies were manually picked and transferred to fresh MEFs. Subsequently, iPSC cultures were passaged either manually or enzymatically with dispase (GIBCO). Control iPSCs were obtained from the ESC/iPSC core of the Children's Hospital of Philadelphia and generated using the Cre-excisable STEMCAA lentiviral vector (Sommer et al., 2010).

Teratoma Formation

MPS VII iPSCs (1×10^6) were resuspended in 140 μl DMEM/F12 and mixed with 60 μl matrigel (BD Biosciences). The cell suspension was injected subcutaneously in NOD/SCID mice (Jackson Labs). Teratomas were removed 6 weeks later and either frozen for immunostaining or embedded in paraffin for H&E staining.

Differentiation and Culture of NSCs

MPS VII and control iPSCs were differentiated based on a protocol for generating long-term self-renewing NSCs from ESCs (Koch et al., 2009). Briefly, iPSC colonies were removed from the MEF feeder layer, and 20% FBS was added in order to generate embryoid bodies. At day 5, the embryoid bodies were attached to poly-ornithine-coated (Sigma) dishes and switched to a minimal neural induction media containing insulin, transferrin, selenium, and fibronectin (Sigma) until neural tube-like structures appear. At day 20, these tube-like structures were manually removed from the surrounding cell mass using a dissecting microscope and transferred to a suspension culture containing N-2 supplement (1:100; GIBCO), basic fibroblast growth factor (bFGF) (10 ng/ml; GIBCO), and EGF (10 ng/ml; Sigma). Cells were trypsinized at day 23 and plated on poly-ornithine/laminin-coated (BD Biosciences) plates in NSC media containing bFGF (10 ng/ml), EGF (10 ng/ml), insulin (20 μg/ml; GIBCO), N-2 (1:100), and B-27 (1:1,000; GIBCO). iPSC-NSCs were passaged 1:2 every 3 to 4 days by trypsinization.

Characterization of iPSC-NSCs

G-banded karyotyping of iPSC-NSCs (p9) was performed by Cell Line Genetics. Terminal in vitro differentiation was carried out in Neurobasal:DMEM/F12 (GIBCO) containing N-2 (1:100), B-27 (1:100), and cyclic AMP (300 ng/ml; Sigma) for 1 month. Quantification of the percentage of undifferentiated and terminally differentiated iPSC-NSCs expressing cell-type specific markers was performed by manual counting of immunofluorescently labeled slides. Percentages are represented as means ± SEM (n = 4).

Gene Transfer in MPS VII iPSC-NSCs

GFP labeling of iPSC-NSCs was achieved using a PiggyBac expression vector containing a puromycin resistance gene (PB-513B-1; Systems Biosciences). The CMV promoter sequence was replaced with the CAG promoter sequence using *SpeI* and EcoRI. *GUSB* was cloned into the PiggyBac plasmid using SmaI sites flanking the *GUSB* cDNA and a *SwaI* site within the multiple cloning site of the PiggyBac plasmid. Blunt-end ligation produced a correction vector as well a mock-correction vector containing *GUSB* in the reverse orientation. For transfection of iPSC-NSCs, we used the Lonza Kit for Mouse Neural Stem Cells according to the manufacturer instructions; 4×10^6 cells were electroporated with 3 μg of the GUSB expression vector or GFP control + 1 μg of the transposase expression plasmid (PB200PA-1; Systems Biosciences) using the Lonza Nucleofector set to program A-33. After allowing the cells a few days to recover, transfected cells were selected with 0.5 μg/ml puromycin for 1 week.

Neonatal NSC Transplantation

Neonatal NOD/SCID mice were cryoanesthetized prior to transplantation. iPSC-NSCs were trypsinized and resuspended in PBS at 50,000 cells per μl; 2 μl of the cell suspension was injected into each lateral ventricle using a pulled glass micropipette. All

procedures were approved by the Institutional Care and Use Committee at the Children's Hospital of Philadelphia.

Adult NSC Transplantation

Prior to injection, 8-week-old NOD/SCID or NOD/SCID/MPS VII mice (breeding stock was a kind gift of Drs. M. Sands and J. Nolta) were anesthetized with isofluorane and secured in a sterotaxic frame (Kopf). Burr holes were drilled into the skull, and 50,000 corrected or mock-corrected cells in 1 μl PBS were infused at a rate of 0.5 μl/min. The striatal coordinates were 0.50 mm caudal to bregma, 1.5 mm left or right of midline, and 3.0 mm ventral to the dural surface.

Adult AAV Injection

Prior to injection, 8-week-old C57BL/6/MPS VII mice (n = 4) were anesthetized with isofluorane and secured in a sterotaxic frame (Kopf). Burr holes were drilled into the skull, and AAV2/1 vector in 1 μl of PBS was infused at a rate of 0.5 μl/min. One hemisphere was injected with AAV2/1-GFP, and the contralateral hemisphere was injected with a 1:1 mixture of AAV2/1-GFP and AAV2/1-GUSB (total of 1×10^{11} vector genomes). Packaging, purification, and titering were performed by The University of Pennsylvania Vector Core as previously described (Passini et al., 2003). The coordinates used for injection were 0.50 mm rostral to bregma, 1.5 mm left or right of midline, and 3.0 mm ventral to the dural surface.

Immunostaining

Brains were embedded in 2% agarose prior to vibratome sectioning and immunostaining; 60 μm coronal sections were stored in PBS + 0.1% Na azide at 4°C until ready for use. Brains were cryoprotected with 30% sucrose prior to embedding in OCT (Tissue-Tek); 20-μm-thick frozen sections were cut using a cryostat (Leica). Vibratome and frozen sections were postfixed in 4% paraformaldehyde and permeabilized in 0.3% Triton X-100. After blocking in 4% goat serum, the sections were incubated in primary antibody containing 1% serum for 1 hr at room temperature. Antibodies used and their concentrations are listed in Table S1. Images were acquired using an epifluorescence microscope (DM6000 B; Leica) or a confocal-scanning laser microscope (FluoView1000; Olympus).

Image Analysis and Statistics

To visualize the distribution of CD68-positive microglia in MPS VII mice following adult iPSC-NSC engraftment, we combined a montage of immunofluorescent images using the photomerge tool in Photoshop CS6 (Adobe). ImagePro Plus 3.0 (Media Cybernetics) was used to identify and dilate all objects with an area greater than 20 pixels. CD68-positive microglia were quantified within 0.25 mm of engrafted iPSC-NSCs. The density of microglia adjacent to corrected and mock-corrected cells was compared by two-tailed t test using Prism 5.0 (Graphpad). Microglia with a CD68-positive area greater than 20 pixels were counted. Frozen sections (20 μm) were quantified for each condition, and data are represented as means ± SEM (n = 7).

β-Glucuronidase Assays

Napthol-AS-BI-β-D-glucuronide was used to determine the presence of GUSB activity in 20-μm-thick frozen sections as previously described (Snyder et al., 1995). For quantitation of β-glucuronidase activity in MPS VII and control NSCs, the fluorescence of hydrolyzed 4-methylumbelliferyl-β-D-glucuronide was measured as previously described (Cervera, 2005). Three independent cultures were quantified, and data are represented as means ± SEM.

SUPPLEMENTAL INFORMATION

Supplemental Information includes five figures and one table and can be found with this article online at http://dx.doi.org/10.1016/j.stemcr.2015.02.022.

AUTHOR CONTRIBUTIONS

T.A.G. designed and performed experiments, collected and analyzed data, and wrote the manuscript. H.C.A. performed experiments, collected data, and contributed to the manuscript. J.H.W. directed the study, designed experiments, and wrote the manuscript. J.H.W. is an inventor on patents for human NSCs.

REFERENCES

Aboody, K., Capela, A., Niazi, N., Stern, J.H., and Temple, S. (2011). Translating stem cell studies to the clinic for CNS repair: current state of the art and the need for a Rosetta stone. Neuron 70, 597–613.

Augustine, E.F., and Mink, J.W. (2013). Enzyme replacement in neuronal storage disorders in the pediatric population. Curr. Treat. Options Neurol. 15, 634–651.

Bergamin, N., Dardis, A., Beltrami, A., Cesselli, D., Rigo, S., Zampieri, S., Domenis, R., Bembi, B., and Beltrami, C.A. (2013). A human neuronal model of Niemann Pick C disease developed from stem cells isolated from patient's skin. Orphanet J. Rare Dis. 8, 34.

Carney, B.J., and Shah, K. (2011). Migration and fate of therapeutic stem cells in different brain disease models. Neuroscience 197, 37–47.

Cervera, M. (2005). Histochemical and fluorometric assays for uidA (GUS) gene detection. Methods Mol. Biol. 286, 203–214.

Chan, E.M., Ratanasirintrawoot, S., Park, I.H., Manos, P.D., Loh, Y.H., Huo, H., Miller, J.D., Hartung, O., Rho, J., Ince, T.A., et al. (2009). Live cell imaging distinguishes bona fide human iPS cells

from partially reprogrammed cells. Nat. Biotechnol. *27*, 1033–1037.

Chaubey, S., and Wolfe, J.H. (2013). Transplantation of CD15-enriched murine neural stem cells increases total engraftment and shifts differentiation toward the oligodendrocyte lineage. Stem Cells Transl. Med. *2*, 444–454.

Conti, L., and Cattaneo, E. (2010). Neural stem cell systems: physiological players or in vitro entities? Nat. Rev. Neurosci. *11*, 176–187.

Elkabetz, Y., Panagiotakos, G., Al Shamy, G., Socci, N.D., Tabar, V., and Studer, L. (2008). Human ES cell-derived neural rosettes reveal a functionally distinct early neural stem cell stage. Genes Dev. *22*, 152–165.

Falk, A., Koch, P., Kesavan, J., Takashima, Y., Ladewig, J., Alexander, M., Wiskow, O., Tailor, J., Trotter, M., Pollard, S., et al. (2012). Capture of neuroepithelial-like stem cells from pluripotent stem cells provides a versatile system for in vitro production of human neurons. PLoS ONE *7*, e29597.

Guha, P., Morgan, J.W., Mostoslavsky, G., Rodrigues, N.P., and Boyd, A.S. (2013). Lack of immune response to differentiated cells derived from syngeneic induced pluripotent stem cells. Cell Stem Cell *12*, 407–412.

Gupta, N., Henry, R.G., Strober, J., Kang, S.M., Lim, D.A., Bucci, M., Caverzasi, E., Gaetano, L., Mandelli, M.L., Ryan, T., et al. (2012). Neural stem cell engraftment and myelination in the human brain. Sci. Transl. Med. *4*, 155ra137.

Guzman, R., Uchida, N., Bliss, T.M., He, D., Christopherson, K.K., Stellwagen, D., Capela, A., Greve, J., Malenka, R.C., Moseley, M.E., et al. (2007). Long-term monitoring of transplanted human neural stem cells in developmental and pathological contexts with MRI. Proc. Natl. Acad. Sci. USA *104*, 10211–10216.

Hofling, A.A., Vogler, C., Creer, M.H., and Sands, M.S. (2003). Engraftment of human CD34+ cells leads to widespread distribution of donor-derived cells and correction of tissue pathology in a novel murine xenotransplantation model of lysosomal storage disease. Blood *101*, 2054–2063.

Kakkis, E., McEntee, M., Vogler, C., Le, S., Levy, B., Belichenko, P., Mobley, W., Dickson, P., Hanson, S., and Passage, M. (2004). Intrathecal enzyme replacement therapy reduces lysosomal storage in the brain and meninges of the canine model of MPS I. Mol. Genet. Metab. *83*, 163–174.

Koch, P., Opitz, T., Steinbeck, J.A., Ladewig, J., and Brüstle, O. (2009). A rosette-type, self-renewing human ES cell-derived neural stem cell with potential for in vitro instruction and synaptic integration. Proc. Natl. Acad. Sci. USA *106*, 3225–3230.

Koso, H., Takeda, H., Yew, C.C., Ward, J.M., Nariai, N., Ueno, K., Nagasaki, M., Watanabe, S., Rust, A.G., Adams, D.J., et al. (2012). Transposon mutagenesis identifies genes that transform neural stem cells into glioma-initiating cells. Proc. Natl. Acad. Sci. USA *109*, E2998–E3007.

Lane, E.L., Björklund, A., Dunnett, S.B., and Winkler, C. (2010). Neural grafting in Parkinson's disease unraveling the mechanisms underlying graft-induced dyskinesia. Prog. Brain Res. *184*, 295–309.

Lee, J.P., Jeyakumar, M., Gonzalez, R., Takahashi, H., Lee, P.J., Baek, R.C., Clark, D., Rose, H., Fu, G., Clarke, J., et al. (2007). Stem cells act through multiple mechanisms to benefit mice with neurodegenerative metabolic disease. Nat. Med. *13*, 439–447.

Lemonnier, T., Blanchard, S., Toli, D., Roy, E., Bigou, S., Froissart, R., Rouvet, I., Vitry, S., Heard, J.M., and Bohl, D. (2011). Modeling neuronal defects associated with a lysosomal disorder using patient-derived induced pluripotent stem cells. Hum. Mol. Genet. *20*, 3653–3666.

Levy, B., Galvin, N., Vogler, C., Birkenmeier, E.H., and Sly, W.S. (1996). Neuropathology of murine mucopolysaccharidosis type VII. Acta Neuropathol. *92*, 562–568.

Maciaczyk, J., Singec, I., Maciaczyk, D., Klein, A., and Nikkhah, G. (2009). Restricted spontaneous in vitro differentiation and region-specific migration of long-term expanded fetal human neural precursor cells after transplantation into the adult rat brain. Stem Cells Dev. *18*, 1043–1058.

Meikle, P.J., Hopwood, J.J., Clague, A.E., and Carey, W.F. (1999). Prevalence of lysosomal storage disorders. JAMA *281*, 249–254.

Meng, X.L., Shen, J.S., Kawagoe, S., Ohashi, T., Brady, R.O., and Eto, Y. (2010). Induced pluripotent stem cells derived from mouse models of lysosomal storage disorders. Proc. Natl. Acad. Sci. USA *107*, 7886–7891.

Mi, R., Luo, Y., Cai, J., Limke, T.L., Rao, M.S., and Höke, A. (2005). Immortalized neural stem cells differ from nonimmortalized cortical neurospheres and cerebellar granule cell progenitors. Exp. Neurol. *194*, 301–319.

Ohmi, K., Greenberg, D.S., Rajavel, K.S., Ryazantsev, S., Li, H.H., and Neufeld, E.F. (2003). Activated microglia in cortex of mouse models of mucopolysaccharidoses I and IIIB. Proc. Natl. Acad. Sci. USA *100*, 1902–1907.

Parente, M.K., Rozen, R., Cearley, C.N., and Wolfe, J.H. (2012). Dysregulation of gene expression in a lysosomal storage disease varies between brain regions implicating unexpected mechanisms of neuropathology. PLoS ONE *7*, e32419.

Park, I.H., Lerou, P.H., Zhao, R., Huo, H., and Daley, G.Q. (2008). Generation of human-induced pluripotent stem cells. Nat. Protoc. *3*, 1180–1186.

Passini, M.A., Lee, E.B., Heuer, G.G., and Wolfe, J.H. (2002). Distribution of a lysosomal enzyme in the adult brain by axonal transport and by cells of the rostral migratory stream. J. Neurosci. *22*, 6437–6446.

Passini, M.A., Watson, D.J., Vite, C.H., Landsburg, D.J., Feigenbaum, A.L., and Wolfe, J.H. (2003). Intraventricular brain injection of adeno-associated virus type 1 (AAV1) in neonatal mice results in complementary patterns of neuronal transduction to AAV2 and total long-term correction of storage lesions in the brains of beta-glucuronidase-deficient mice. J. Virol. *77*, 7034–7040.

Platt, F.M., Boland, B., and van der Spoel, A.C. (2012). The cell biology of disease: lysosomal storage disorders: the cellular impact of lysosomal dysfunction. J. Cell Biol. *199*, 723–734.

Simonato, M., Bennett, J., Boulis, N.M., Castro, M.G., Fink, D.J., Goins, W.F., Gray, S.J., Lowenstein, P.R., Vandenberghe, L.H., Wilson, T.J., et al. (2013). Progress in gene therapy for neurological disorders. Nat. Rev. Neurol. *9*, 277–291.

Snyder, E.Y., and Wolfe, J.H. (1996). Central nervous system cell transplantation: a novel therapy for storage diseases? Curr. Opin. Neurol. *9*, 126–136.

Snyder, E.Y., Taylor, R.M., and Wolfe, J.H. (1995). Neural progenitor cell engraftment corrects lysosomal storage throughout the MPS VII mouse brain. Nature *374*, 367–370.

Sommer, C.A., Sommer, A.G., Longmire, T.A., Christodoulou, C., Thomas, D.D., Gostissa, M., Alt, F.W., Murphy, G.J., Kotton, D.N., and Mostoslavsky, G. (2010). Excision of reprogramming transgenes improves the differentiation potential of iPS cells generated with a single excisable vector. Stem Cells *28*, 64–74.

Tabar, V., Panagiotakos, G., Greenberg, E.D., Chan, B.K., Sadelain, M., Gutin, P.H., and Studer, L. (2005). Migration and differentiation of neural precursors derived from human embryonic stem cells in the rat brain. Nat. Biotechnol. *23*, 601–606.

Takahashi, K., and Yamanaka, S. (2006). Induction of pluripotent stem cells from mouse embryonic and adult fibroblast cultures by defined factors. Cell *126*, 663–676.

Taylor, R.M., and Wolfe, J.H. (1997). Decreased lysosomal storage in the adult MPS VII mouse brain in the vicinity of grafts of retroviral vector-corrected fibroblasts secreting high levels of beta-glucuronidase. Nat. Med. *3*, 771–774.

Wada, R., Tifft, C.J., and Proia, R.L. (2000). Microglial activation precedes acute neurodegeneration in Sandhoff disease and is suppressed by bone marrow transplantation. Proc. Natl. Acad. Sci. USA *97*, 10954–10959.

Walton, R.M., and Wolfe, J.H. (2007). Abnormalities in neural progenitor cells in a dog model of lysosomal storage disease. J. Neuropathol. Exp. Neurol. *66*, 760–769.

Walton, R.M., Magnitsky, S.G., Seiler, G.S., Poptani, H., and Wolfe, J.H. (2008). Transplantation and magnetic resonance imaging of canine neural progenitor cell grafts in the postnatal dog brain. J. Neuropathol. Exp. Neurol. *67*, 954–962.

Watson, D.J., Kobinger, G.P., Passini, M.A., Wilson, J.M., and Wolfe, J.H. (2002). Targeted transduction patterns in the mouse brain by lentivirus vectors pseudotyped with VSV, Ebola, Mokola, LCMV, or MuLV envelope proteins. Mol. Ther. *5*, 528–537.

Wolfe, J.H., and Sands, M.S. (1996). Murine mucopolysaccharidosis type VII: a model system for somatic gene therapy of the central nervous system. In Gene Transfer into Neurones, towards Gene Therapy of Neurological Disorders, P. Lowenstein and L. Enquist, eds. (Essex: J. Wiley and Sons), pp. 263–274.

Wright, L.S., Prowse, K.R., Wallace, K., Linskens, M.H., and Svendsen, C.N. (2006). Human progenitor cells isolated from the developing cortex undergo decreased neurogenesis and eventual senescence following expansion in vitro. Exp. Cell Res. *312*, 2107–2120.